

Manipulation of the magnetic state of a small ferromagnetic particle by means of nonlocal spin-injection techniques (invited)

Y. Otani^{a)} and T. Kimura

Institute for Solid State Physics, University of Tokyo, 5-1-5 Kashiwanoha, Chiba 277-8581, Japan and Frontier Research System (FRS) RIKEN, 2-1 Hirosawa, Wako Saitama 351-0198, Japan

(Presented on 2 November 2005; published online 18 April 2006)

Nonlocal spin-valve configuration is used for spin current injection into a nanoscale ferromagnetic particle to reverse its magnetization. The nonlocal spin injection aligns the magnetization of the nanoscale particle along the spin injector, whereas the reverse switching is hardly observed up to the available maximum exciting current of about 15 mA. This asymmetric behavior implies the presence of asymmetric barrier formed in the vicinity of the interface. The magnitude of the essential spin current for the reversal is determined to be about 160 μA , on the reasonable order of magnitude compared with the experimental values for conventional pillar structures. © 2006 American Institute of Physics. [DOI: 10.1063/1.2162031]

I. INTRODUCTION

The current-induced magnetic switching is a key phenomenon for future spin electronic devices including a next generation magnetic random access memory. Slonczewski¹ and Berger² have separately shown that the responsible switching mechanism is attributable to the spin current-induced torque exerted on the localized spin (*spin transfer*). This implies that the spin current is essential for the spin-injection-induced magnetization reversal. Most of the spin-transfer devices studied up to now consists of vertical multilayered nanopillars in which typically two magnetic layers are separated by a nonmagnetic metal layer.³⁻⁵ In such vertical structures, the spin current is always accompanied by the charge current, by which undesirable Joule heat is generated in the heart of the device.

Our recent experiments have revealed that the spin currents are preferably absorbed into an additionally connected metallic wire with a small spin resistance.^{5,6} This indeed means that the spin current with no net charge flow can be selectively injected into a ferromagnetic particle with a small spin resistance such as a Permalloy (Py) particle replaced by the wire. This spin current may contribute to the magnetization reversal. To test this idea, a nonlocal spin-injection device is designed as in Fig. 1(a) in which a charge current is deflected toward either right or left at the cross so that, unlike the direct spin-injection device [Fig.1(b)], only the spin current can reach the Py nanoparticle indicated as F_2 .

II. EXPERIMENTAL PROCEDURES

Multiterminal spin-injection device used in this study is fabricated by means of conventional *e*-beam lithography followed by a lift-off process. Figures 2(a) and 2(b) show the scanning electron microscope (SEM) ordinary and magnified images of a fabricated device. The device consists of a micron-sized large Py pad 30 nm thick, a Cu cross 100 nm wide and 80 nm thick, and a Py nanoparticle 50 nm wide,

180 nm long, and 6 nm thick. A gold wire 100 nm wide and 40 nm thick is connected to the Py particle to minimize the effective spin resistance to obtain high spin current absorption into the Py particle.⁶ The magnetic field is applied along the easy axis of the Py particle. Note that the dimensions of Py pad and Cu wires are chosen large enough so that the exciting charge current can flow up to 15 mA ($\sim 10^8$ A/cm²) through them. Py layer is grown by using an electron-beam evaporator with a base pressure of 2×10^{-9} Torr. The Cu and Au wires are deposited by a resistance heating evaporator with a base pressure of 3×10^{-8} Torr. The interface between the Py and Cu and that between the Py and Au are well cleaned by Ar-ion milling prior to each deposition. Very low resistance of the interface assures a good Ohmic contact. The distance between the Py pad and the particle is 400 nm. The resistivities of Py and Cu wires are respectively 10.2 and 1.14 $\mu\Omega$ cm at 77 K. All the measurements are performed at 77 K by means of conventional lock-in technique.

III. RESULTS AND DISCUSSION

Firstly we discuss *the spin sink effect* that is the spin current absorption into the additionally connected metallic wire. We have demonstrated that the spin current distribution can be calculated by the model base on the spin-resistance circuit and that the spin current favors flowing into the region which has relatively small spin resistance.^{6,7} The spin resistance is given by $2\rho_i\lambda_i/(1-\alpha_i^2)S_i$, where ρ_i , λ_i , α_i , and S_i are the resistivity, spin-diffusion length, spin polarization,

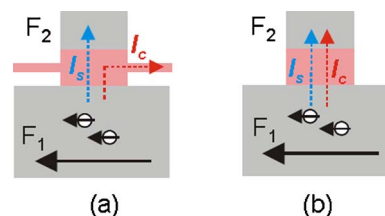


FIG. 1. (Color online) Schematic illustrations of (a) nonlocal spin injection and (b) local spin injection.

^{a)}Electronic mail: yotani@issp.u-tokyo.ac.jp

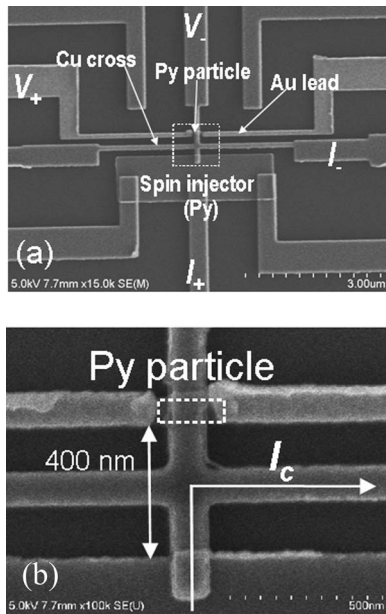


FIG. 2. (a) SEM image of the fabricated lateral spin-injection device and (b) magnified image around the Py particle.

and the cross section of the wire. For example, the spin resistance R_S^{Cu} for the Cu wire with the cross section S_i of $100 \times 80 \text{ nm}^2$ can be calculated as 2.85Ω . We take the value of $1 \mu\text{m}$ obtained in our previous experiments for the spin-diffusion length of the Cu wire.⁷ The effective cross section for the spin-resistance of the Py particle in Fig. 2(b) is given by the junction area between the Py particle and the Cu wire because the spin diffusion length of the Py is very short. We then obtain the spin resistance R_S^{Py} for the Py particle as 0.08Ω . The parameters used for this calculation are the Py spin polarization $\alpha_{\text{Py}}=0.2$ and the Py spin diffusion length $\lambda_{\text{Py}}=2 \text{ nm}$ in Ref. 7. Important is that R_S^{Py} is about two orders of magnitude smaller than R_S^{Cu} . Therefore, the Py particle favors absorbing the spin current although the particle is electrically floating, meaning that the Py particle act as *the spin sink*. Such absorption can be employed as a method to inject the spin current without a net charge flow.

To begin with, the nonlocal spin-valve (NLSV) measurements are performed to understand the magnetization process of the Py nanoparticle with respect to the Py pad in our devices. Figures 3(a) and 3(b), respectively, show the magnetic-field-dependent NLSV signals with current excitation on either right- or left-hand side. In both cases, we can see clear changes in NLSV signals of $0.18 \text{ m}\Omega$ for the right and $0.19 \text{ m}\Omega$ for the left, corresponding to the relative magnetic switching of the Py pad and the particle, from parallel (*P*) to antiparallel (*AP*) states and vice versa. The difference between the two values is due to inhomogeneous distribution of the spin current. These results prove that the spin current generated from the Py pad reaches the Py particle. It should be noted that both of the measured NLSV signals are smaller than the values expected from our previous experiments.⁷⁻⁹ As will be mentioned later, this is because the Py particle used in the present study seems to have smaller spin resistance than the Py wire used in our ordinary lateral spin-valve experiments.⁷⁻⁹

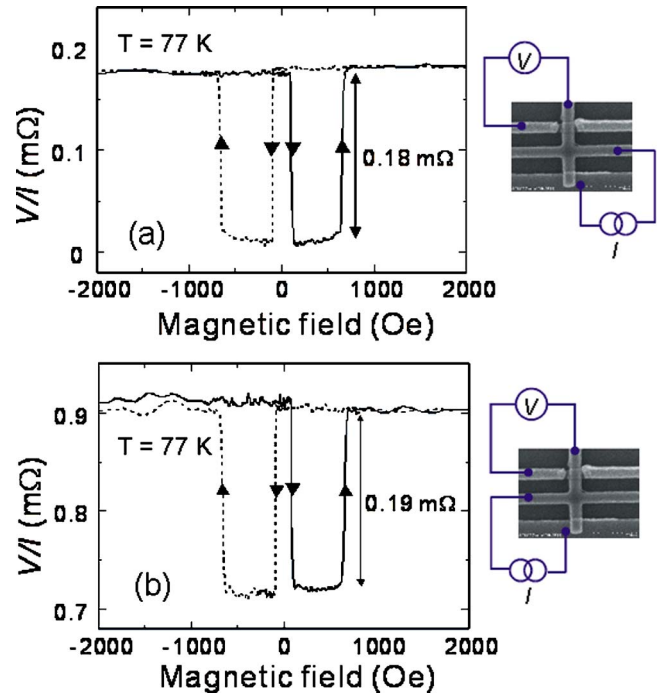


FIG. 3. (Color online) Nonlocal spin-valve signal measured at 77 K with current excitation on the right-hand side (a) and on the left-hand side (b) together with corresponding schematic probe configurations.

We first examine the effect of the nonlocal spin injection into the Py particle using the probe configuration, as shown in the inset of Fig. 3(a). Before performing the nonlocal spin injection, the magnetic configuration is set in the AP state by controlling the external magnetic field. The nonlocal spin injection is then performed by applying large pulsed currents up to 15 mA with the same current probes for the NLSV measurement in the absence of magnetic field. It should be noted that the current pulse is triangular shaped with variable amplitude and a fixed duration of 1 s. After the nonlocal spin injection, the NLSV signal is successively measured to determine the magnetic state of the Py particle with respect to the pad. In this way, as shown in Figs. 4(a) and 4(b), the NLSV signals after the nonlocal spin injection are obtained as a function of the amplitude of the pulsed current. As in Fig. 4(a), when the magnitude of the pulsed current is increased positively in the AP state, no signal change is observed up to 15 mA. On the other hand, for the negative scan, the abrupt signal change is observed at -14 mA . The change in resistance at -14 mA is $0.18 \text{ m}\Omega$, consistent with the change in NLSV signal from AP to *P* states. The magnetization direction of the Py particle is confirmed to be parallel to the Py pad by further sweeping the magnetic field with measuring the NLSV signal. After the transition from the AP to *P* states, the current is positively increased in the *P* state. However, we observe no signal change up to the pulsed current amplitude of 15 mA. In this measurement, there are two equivalent AP states in which the magnetization of the Py particle directs towards either left or right as can be understood in the inset of Fig. 4(a). Both AP states are found to transform into the *P* state in the same manner.

We can exclude a possibility that the magnetization of the Py particle is switched by the current-induced Oersted

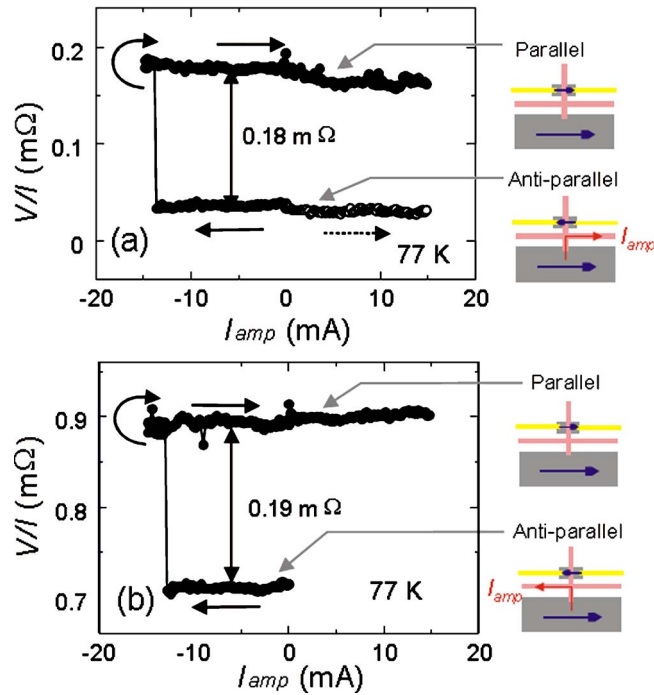


FIG. 4. (Color online) The NLSV signal measured after the pulsed nonlocal spin current injection as a function of the current amplitude with different probe configurations excited by the pulsed current applied on the right-hand side (a) and on the left-hand side (b).

field as follows. In the probe configuration for the nonlocal spin injection, the charge current passing through the Cu cross induces the Oersted field. However, the induced Oersted fields have components mostly normal to the substrate which do not contribute to the magnetization reversal of the Py particle since the demagnetizing field of nearly 1 T is far bigger than the Oersted field.

The similar spin-injection measurement is performed with a current excitation on the left-hand side, as shown in the inset of Fig. 3(b). Similarly the clear transition from the AP to *P* states is observed although the reverse *P* to AP transition does not appear. For this experiment, the switching occurs at -13.3 mA slightly smaller than that of the previous configuration. This suggests that the larger spin accumulation takes place at the interface leading to the larger spin current than in the previous configuration in Fig. 3(a). In this probe configuration, the distribution of the Oersted field is different from the previous experiment. No remarkable difference is observed between the two experiments. This also supports that the observed AP to *P* transition is not originated by the Oersted field. It should be noted here that for both cases the Oersted field exerted normal to the substrate causes a deviation from the collinear magnetic configuration between Py pad and particle,¹⁰ and this may facilitate the magnetization switching of the Py particle due to the spin torque, resulting in the reduction of the switching current.

We examine the magnitude of injected spin current into the Py particle in the AP state. When the electrons are injected from the Py pad into the Cu wire (negative current), the nonequilibrium magnetization arises over the spin-diffusion length of the Cu wire, parallel to the magnetization of the Py pad. The continuity of the chemical potential at the

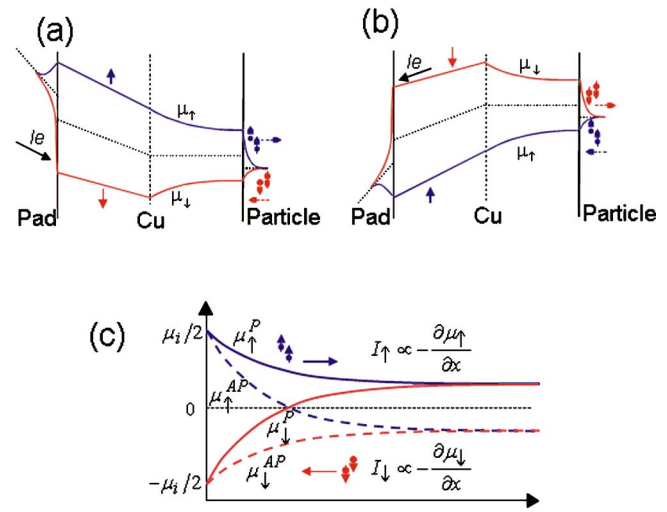


FIG. 5. (Color online) Schematic illustrations of (a) the induced chemical potential for the negative current injection in the antiparallel configuration and (b) that for the positive current injection in the parallel configuration. (c) Spin-dependent chemical potential inside the Py particle in parallel (antiparallel) to the Py pad in the negative current. The direction of the injected spin current depends on the polarity of the current and does not depend on the magnetization configuration between the Py pad and the particle.

interface also brings about the spin splitting in the Py particle, as shown in Figs. 5(a)–5(c). The spin-dependent chemical potential of the Py particle whose magnetization is antiparallel to the magnetization of the Py pad is given by^{11–13}

$$\mu_{\uparrow} = \mu_i \left(\frac{\alpha_{\text{Py}}}{2} - \frac{1 + \alpha_{\text{Py}}}{2} e^{-(x/\lambda_{\text{Py}})} \right) \quad (1)$$

and

$$\mu_{\downarrow} = \mu_i \left(\frac{\alpha_{\text{Py}}}{2} + \frac{1 - \alpha_{\text{Py}}}{2} e^{-(x/\lambda_{\text{Py}})} \right). \quad (2)$$

Defining the spin current as $I_S = I_{\uparrow} - I_{\downarrow} = -(S_{\text{Py}}\sigma_{\uparrow}/e)(\partial\mu_{\uparrow}/\partial x) + (S_{\text{Py}}\sigma_{\downarrow}/e)(\partial\mu_{\downarrow}/\partial x)$ yields the injected (absorbed) total spin current into the Py particle,

$$I_S = \frac{(1 - \alpha_{\text{Py}}^2)\sigma_{\text{Py}}S}{2e\lambda_{\text{Py}}} \mu_i = \frac{\mu_i}{eR_S^{\text{Py}}}. \quad (3)$$

The magnitude of the injected spin current can be deduced from the intensity of the NLSV signal by using Eq. (3). The relation between the induced spin splitting in the chemical potential μ_i at the interface and the obtained NLSV signal R_{NLSV} is given by $\mu_i = e i_c R_{\text{NLSV}} / \alpha_{\text{Py}}$. Here, i_c is the applied charge current for the measurement. Therefore, when a pulsed current with amplitude of I_{amp} is applied, the injected spin current I_S^{inj} into the Py particle can be calculated as

$$I_S^{\text{inj}} = \frac{\mu_i}{eR_S^{\text{Py}}} = \frac{R_{\text{NLSV}} I_{\text{amp}}}{\alpha_{\text{Py}} R_S^{\text{Py}}}. \quad (4)$$

As mentioned above, the spin resistance of the Py particle is 0.08Ω . When we use the parameters determined in previous experiments,^{6–8} we obtain the injected spin current as $158 \mu\text{A}$ for $I_{\text{amp}} = -14$ mA. The value can be compared with that of conventional pillar structures consisting of Py based

CPP devices.^{14,15} The observed spin current for switching the free layer from the AP to *P* states in the vertical structures is about 200 μA , slightly larger than the value obtained in the present experiment. As mentioned above, the Py nanoparticle exhibits the smaller NLSV signal than that of the ordinary NLSV experiment with the same injector-detector distance. We believe that this is caused by the lower quality of the Py nanoparticle than the wire in our previous lateral spin-valve experiments. In the Py nanoparticle, the surface oxidation is more pronounced than the conventional devices because of the small sample dimensions, large surface volume ratio. Such effects reduce the spin polarization and the spin-diffusion length of the Py particle. This causes the reduction of the spin resistance, and lowers the estimated spin splitting voltage at the interface. The actual injected spin current may therefore be larger than the above calculation.

Similar analysis for the positive current reveals that the spin current with the same magnitude and the opposite polarity is injected into the Py particle as in Fig. 5(b). The spin current induced by nonlocal spin injection with the positive current should lead the Py particle's magnetization into the AP state. This transition, however, is not observed in the present experiment. Although the concrete reason is not clear, conceivable explanations for this discrepancy may be as follows. One is a bias-dependent spin polarization of the Py pad. In general, the spin polarization should be independent of the current passing through the interface of the Ohmic junction. However, it is not true once very thin oxide layer is formed at the interface between the Py pad and Cu cross during fabrication process. There is a possibility to have the thin oxide layer at the interface since our device is exposed to the air during the process. Such an oxidized layer may provide an asymmetric barrier especially at high current density. Therefore, we have to take into account an asymmetric spin injection into or out of the Py pad. When the electron is injected from the Cu wire into the Py pad, the spin polarization drastically diminishes from the zero-bias value with increasing the applied bias voltage,¹⁶ thus reducing the injected spin current into the Py particle. On the contrary, the spin polarization exhibits only small reduction when the electron is injected from the Py pad into the Cu wire. In this way, our asymmetric reversal of the Py nanoparticle can be explained. Another possibility is a tiny magnetic impurity in the Cu wire near the interface. The spin-diffusion length of the Cu wire with the magnetic impurity is known to depend on the angle between the direction of the impurity magnetic moment and that of the injected spin.¹⁷ When the direction of

the injected spin is antiparallel to the moment of the magnetic impurity, the spin-diffusion length is shorter than that at the parallel alignment because of the reorientation of the magnetic moment of the conduction electron spin to the direction of that of the magnetic impurity. The magnetic impurity in the Cu wire may be parallel to the magnetization of the Py pad because of the exchange interaction. In this case, when the electron is injected from the Cu wire to the Py pad (corresponding to the positive current), the spin-diffusion length is shorter than that of the negative current. This asymmetric transport also explains our experimental results.

IV. CONCLUSIONS

In conclusion, we have fabricated the multiterminal lateral spin-injection devices configured for the nonlocal spin-injection-induced magnetization switching of the Py particle. We succeeded in switching the magnetization of the Py particle from the AP to the *P* states by nonlocal spin injection although we could not realize the *P* to AP switching. The conceivable reasons for this asymmetry are discussed. The value of the switching current obtained from the experiment is reasonable compared with the values estimated from the conventional pillar devices. In order to flip the magnetization of the Py particle in both directions, further optimization of the device structure is needed.

¹J. C. Slonczewski, *J. Magn. Magn. Mater.* **159**, L1 (1996).

²L. Berger, *Phys. Rev. B* **54**, 9353 (1996).

³J. Grollier *et al.*, *Appl. Phys. Lett.* **78**, 3663 (2001).

⁴F. J. Albert, N. C. Emley, E. B. Myers, D. C. Ralph, and R. A. Buhrman, *Phys. Rev. Lett.* **89**, 226802 (2002).

⁵F. J. Albert, J. A. Katine, R. A. Buhrman, and D. C. Ralph, *Appl. Phys. Lett.* **77**, 3809 (2000).

⁶T. Kimura, J. Hamrle, and Y. Otani, *Phys. Rev. B* **72**, 014461 (2005).

⁷T. Kimura, J. Hamrle, Y. Otani *et al.*, *Appl. Phys. Lett.* **85**, 3795 (2004).

⁸T. Kimura, J. Hamrle, and Y. Otani (unpublished).

⁹M. Johnson and R. H. Silsbee, *Phys. Rev. Lett.* **55**, 1790 (1985).

¹⁰B. Ozyilmaz, A. D. Kent, D. Monsma, J. Z. Sun, M. J. Rooks, and R. H. Koch, *Phys. Rev. Lett.* **91**, 067203 (2003).

¹¹F. J. Jedema, A. T. Filip, and B. J. van Wees, *Nature (London)* **410**, 345 (2001); F. J. Jedema, M. S. Nijboer, A. T. Filip, and B. J. van Wees, *Phys. Rev. B* **67**, 085319 (2003).

¹²S. Takahashi and S. Maekawa, *Phys. Rev. B* **67**, 052409 (2003).

¹³P. C. van Son, H. van Kempen, and P. Wyder, *Phys. Rev. Lett.* **58**, 2271 (1987).

¹⁴I. N. Krivorotov, N. C. Emley, J. C. Sankey, S. I. Kiselev, D. C. Ralph, and R. A. Buhrman, *Science* **307**, 228 (2005).

¹⁵S. Urzhdin, N. O. Birge, W. P. Pratt, Jr., and J. Bass, *Phys. Rev. Lett.* **91**, 146803 (2003).

¹⁶S. O. Valenzuela, D. J. Monsma, C. M. Marcus, V. Narayanamurti, and M. Tinkham, *Phys. Rev. Lett.* **94**, 196601 (2005).

¹⁷C. Heide, *Phys. Rev. B* **65**, 054401 (2002).